Oxygen Exchange in the Isolated, Arrested Guinea Pig Heart: Theoretical and Experimental Observations

David A. Mawson,* Peter J. Hunter,* Diane N. Kenwright,‡ and Denis S. Loiselle‡
Departments of *Engineering Science, and ‡Physiology, University of Auckland, Auckland, New Zealand

ABSTRACT A model of oxygen transport in perfused myocardial tissue is presented. Steady-state conditions are assumed in order to mimic the metabolic rate of the arrested heart. The model incorporates Michaelis-Menten dependence of mitochondrial oxygen consumption, oxymyoglobin saturation and oxyhemoglobin saturation on oxygen partial pressure (PO_2). The transport equations model both the advective supply of oxygen via the coronary circulation and the diffusive exchange of oxygen between tissues and environment across the epicardial and endocardial surfaces. The left ventricle is approximated by an axisymmetric prolate spheroid and the transport equations solved numerically using finite element techniques. Solution yields the PO_2 profile across the heart wall. Integration of this profile yields the simulated rate of metabolic oxygen uptake determined according to the Fick principle. Correction for the diffusive flux of oxygen across the surfaces yields the simulated true metabolic rate of oxygen consumption. Simulated values of oxygen uptake are compared with those measured experimentally according to the Fick principle, using saline-perfused, Langendorff-circulated, K^+-arrested, guinea pig hearts. Four perfusion variables were manipulated: arterial PO_2, environmental PO_2, coronary flow and perfusion pressure. In each case agreement between simulated and experimentally determined rates of oxygen consumption gives confidence that the model adequately describes the advective and diffusive transport of oxygen in the isolated, arrested, saline-perfused heart.

INTRODUCTION

The function of the heart is critically dependent on a continuous supply of oxygen. In the classical view, oxygen transport is admitted to have both diffusive and advective components, but these are assumed to be confined to anatomically distinct compartments of the blood delivery system. Thus, the arterial and venous networks of the coronary circulation are commonly presumed to be impervious to oxygen, whereas diffusive exchange with the tissues is traditionally confined to the capillaries. An implicit extension of this assumption is that diffusive oxygen flux across either the epicardial or endocardial surfaces of the heart is negligible. It is this assumption that allows application of the Fick Principle to calculate the rate of oxygen consumption of the heart.

A recent investigation (Loiselle, 1989) has shown the assumption of zero boundary flux of oxygen to be seriously in error. In that investigation, a simple algebraic model was developed to account for the experimental observation that the apparent rate (and even *direction*) of oxygen consumption, calculated via the Fick Principle (i.e., as the product of flow and the arteriovenous difference of oxygen content), is sensitive to the environmental partial pressure of oxygen. More recently, van Beek et al. (1992) have utilised a modified version of the equation describing bioheat transfer (Pennes, 1948) to model oxygen transport and exchange in the myocardium. Their analytical, single-field description (in which blood vessels and myocardial tissue are assumed to be a single homogeneous medium) models the left ventricular wall as a rectangular slab in which oxygen is both supplied and consumed at every point, is free to exchange with the environment, and is consumed at a rate independent of its partial pressure (PO_2).

In the current investigation, we extend the van Beek model in several substantial ways. A more general two-field model (with separate PO_2 fields for blood vessels and myocardial tissue) is presented, in which advection is confined to that fraction of the myocardium representing the coronary circulation. The heart is initially modeled as a radially symmetric, prolate spheroidal shell in order to ascertain the magnitude of longitudinal PO_2 gradients. Simulations showing that these are negligible allow reversion to the simpler slab model. The rate at which oxygen is consumed by the tissues is assumed to depend on its partial pressure, according to Michaelis-Menten behavior, whereas its diffusive transport is assumed to be myoglobin-facilitated. This more realistic model is solved by finite element techniques yielding numerical rather than analytical solutions. These solutions are compared with experimentally determined measurements of the rate of oxygen consumption of isolated, Langendorff-perfused guinea pig hearts that have been arrested by elevation of the K^+ concentration of the saline perfusate. Saline perfusion greatly simplifies the description of advective oxygen supply, whereas the arrested state offers the advantage of a steady-state rate of myocardial oxygen consumption, unperturbed by beat-to-beat variation.

Received for publication 24 June 1993 and in final form 12 November 1993.

Address reprint requests and all correspondence to D. S. Loiselle, Department of Physiology, School of Medicine, University of Auckland, Auckland, New Zealand.

Dr Kenwright's current address is: Division of Anatomic Pathology, Wellington Hospital, Wellington, New Zealand.

Preliminary reports of this research were presented to the International Society for Heart Research: Sapporo & Kobe, Japan, May 1992 and Melbourne, Australia, August 1992.

0006-3495/94/03/789/12 $2.00

Our results suggest that previous investigations have overestimated the effects of coronary flow and vasodilation on the rate of oxygen consumption because of the hitherto unrecognized diffusive loss of oxygen from an isolated, perfused heart to its surrounds.

GLOSSARY

Simulation

Q (nmol s^{-1})	oxygen source or sink per unit volume
$\mathbf{u}$ (mm s^{-1})	blood velocity
c (nmol mm^{-3})	oxygen concentration
σ_t (nmol mm^{-3} kPa^{-1})	oxygen solubility of muscle tissue
σ_p (nmol mm^{-3} kPa^{-1})	oxygen solubility of coronary perfusate
D_t (mm^2 ks^{-1})	diffusion coefficient of oxygen in muscle tissue
D_p (mm^2 ks^{-1})	diffusion coefficient of oxygen in the perfusate
D_{Mb} (mm^2 ks^{-1})	diffusion coefficient of myoglobin
k_t (ks^{-1})	coefficient of oxygen exchange from perfusate to tissue
k_p (ks^{-1})	coefficient of oxygen exchange from tissue to perfusate
PO_2 (kPa)	partial pressure of oxygen
P_a, P_t, P_{env} (kPa)	arterial, tissue, environmental PO_2
M, F, H	relations describing dependence on PO_2 of mitochondrial oxygen consumption, myoglobin saturation, and hemoglobin saturation, respectively
m, f, h	normalised M, F, and H relations, respectively
m_{max}, f_{max}, h_{max}	factors scaling the M, F, and H relations, respectively
$\dot{V}^s$ (μl s^{-1} mm^{-3})	simulated rate of coronary flow
$\dot{V}^s_{O_2}$ (nmol s^{-1} cm^{-3})	simulated rate of oxygen uptake computed according to the Fick Principle
L (mm)	slab thickness
t (s)	time
x, y, z (mm)	coordinates of rectangular coordinate system
λ, μ, θ	coordinates of prolate spheroidal coordinate system
d (mm)	focus of prolate spheroidal coordinate system
ξ	normalized finite element coordinate ($0 \leq \xi \leq 1$)
$\bar{P}_t$ (kPa)	mean tissue PO_2
$\bar{P}_e$ (kPa)	mean PO_2 within an element
R	relative volume of coronary vascular system
$\bar{m}$ (nmol s^{-1} cm^{-3})	simulated rate of oxygen consumption of the heart
J (nmol s^{-1} cm^{-3})	simulated net flux of oxygen across the endocardial and epicardial surfaces

Experimental Measurement

$\dot{V}^m$ (μl s^{-1} g^{-1})	measured rate of coronary flow
a, v (nmol μl^{-1})	arterial, venous oxygen content of coronary perfusate
$\dot{V}^m_{O_2}$ (nmol s^{-1} g^{-3})	measured cardiac oxygen uptake, calculated according to the Fick Principle

METHODS

Experimental

The method of Langendorff perfusion of isolated guinea pig hearts has been described in detail previously (Loiselle, 1989). Briefly, hearts were excised and retrogradely perfused through the distal stump of the aorta. A glass cannula was inserted into the right ventricle, via the pulmonary artery, to collect the coronary venous drainage that returns to the right atrium via the coronary sinus. Saline perfusion could be performed, using a roller pump, either at constant pressure (the standard condition) or at constant flow. The temperature and PO_2 of the perfusate could be independently varied. The heart was enclosed in a glass chamber that was vigorously flushed with a stream of gas of variable PO_2. Timed collection of the coronary venous effluent provided an estimate of coronary flow. The oxygen content of arterial and venous samples was determined, in duplicate, using a CAVITRON/LEX O_2 CON-K oxygen analyzer (Cavitron International Medical Sales, Anaheim, CA). The experimentally measured rate of oxygen uptake by the heart ($\dot{V}^m_{O_2}$) was calculated as the product of the measured rate of coronary flow ($\dot{V}^m$) and the arteriovenous difference of oxygen content ($a - v$)

$$\dot{V}^m_{O_2} = \dot{V}^m \cdot (a - v). \quad (1)$$

Hereafter, $\dot{V}^m_{O_2}$ is expressed in units of nmol·s^{-1} normalized per gram wet weight of myocardial tissue. By way of contrast, simulated values of oxygen exchange (i.e., those predicted by solution of the mathematical model) are normalized per cm^3 of tissue. These units are nearly equivalent, given a tissue density of 1.05 g·cm^{-3} (Hill, 1965). PO_2 is expressed in SI units (kPa), where 1 kPa oxygen partial pressure is approximately equivalent to 1% O_2 (101.325 kPa ≡ 1 atm ≡ 100%), except that correction must be made for the saturation vapor pressure of water (6.27 kPa at 37°C).

The standard perfusate was a modified Krebs-Henseleit solution of the following composition (mM): NaCl 118, KCl 4.8, $MgSO_4$ 1.18, KH_2PO_4 1.18, $NaHCO_3$ 24.8, $CaCl_2$ 2.54, and glucose 10, to which was added insulin (10 units/litre) and *Haemaccel* (Hoechst NZ Ltd., Auckland) (20 ml/l). It was gassed with 95% O_2/5% CO_2, and the temperature maintained at 37°C unless otherwise specified. In selected experiments the coronary vasodilatory agent adenosine (2 mM) was added to the perfusate.

Four series of experiments were performed. In each experimental series, only a single variable (arterial PO_2, ambient PO_2, coronary flow, or perfusion pressure) was altered while the same protocol was followed. First, the rate of oxygen uptake of the spontaneously beating heart was determined. The heart was then arrested by elevation of the KCl concentration of the saline perfusate to give a final K^+ concentration of 20 mM. The rate of oxygen uptake of the K^+-arrested heart was then sequentially measured under *each* level of the variable of interest (all seven values of arterial PO_2, for example). For any given heart, the order of presentation of these various levels was dictated by the constraints of Latin Squares (of the appropriate order) arranged to achieve full balance. The arrested heart was then allowed to resume beating by return to the standard (i.e., low K^+) perfusate. If either the spontaneous heart rate or the rate of oxygen uptake failed to recover to at least 80% of its corresponding pre-arrest value, then the results of that particular experiment were discarded. This occurred in fewer than 10% of the cases. Experimental results are presented as mean ± SE.

Throughout the following, we maintain a distinction between *oxygen uptake* and *oxygen consumption*. The former is commonly assessed experimentally by application of the Fick principle. It includes the oxygen consumption (i.e., the rate at which O_2 is converted to CO_2 in the mitochondria) as well as any other process whereby oxygen disappears from (or appears in) the coronary supply vessels. Although it is desired to measure the rate of oxygen *consumption*, only the rate of oxygen *uptake* can be unambiguously observed experimentally. In the theoretical model that follows, the distinction between the two variables is made explicit.

Theoretical

The derivation of the general equations used to represent the oxygen transport processes is based on the work of Hunter and Smaill (1988) and takes as its starting point the advection-diffusion equation

$$\frac{\partial c}{\partial t} + \mathbf{u} \cdot \nabla c - D\nabla^2 c = Q. \tag{2}$$

In this equation (in which vector quantities are signified by boldface type) c is the concentration of oxygen and D is the oxygen diffusion coefficient which, in the absence of experimental evidence to the contrary, is assumed to be isotropic and spatially homogeneous; $\mathbf{u}$ is the velocity of the blood, and Q represents the sum of all sources and sinks of oxygen.

It is assumed that, within the heart, the sole sites of oxygen consumption lie within the cardiac myocytes; so it follows that $Q = 0$ in the extracellular regions. The general advective term involving the blood velocity vector, $\mathbf{u}$, applies only to the coronary circulation. When modeling processes at the microscopic level, detailed knowledge of the spatial organization of the coronary vessels and the myocytes is necessary. At the macroscopic level, *detailed* evaluation of the advective term is not feasible, so we consider, instead, a spatially uniform oxygen exchange between the microcirculation and the myocytes.

Because oxygen diffusion occurs only if there is a gradient of its partial pressure (Forster, 1964), it is necessary to consider the variation of the oxygen partial pressure field, $P(x, t)$, rather than the oxygen concentration field, $c(x, t)$. The two quantities are related by the oxygen solubility (σ), which varies among media but, again in the absence of experimental evidence to the contrary, is assumed to have no spatial dependence within a medium

$$c(x) = \sigma P(x) \tag{3}$$

With this background, the governing equations of the model can now be presented. There are two equations, coupled by exchange coefficients, which describe the delivery and consumption of oxygen within the myocardium. In this two-field formulation we include the non-linear relations describing myoglobin-facilitated oxygen diffusion and mitochondrial oxygen consumption within the myocytes, as well as hemoglobin-facilitated advection of oxygen in the blood. Note that P_t is the partial pressure of oxygen in the muscle tissue, whereas P_p represents the partial pressure of oxygen in the perfusate.

$$\sigma_t \frac{\partial P_t}{\partial t} + \frac{\partial F(P_t)}{\partial t} - \sigma_t D_t \nabla^2 P_t = \sigma_t k_t (P_p - P_t) + D_{Mb}\nabla^2 F(P_t) - M(P_t) \tag{4}$$

$$\sigma_p \frac{\partial P_p}{\partial t} + \frac{\partial H(P_p)}{\partial t} + \sigma_p \mathbf{u} \cdot \nabla P_p - \sigma_p D_p \nabla^2 P_p = -\mathbf{u} \cdot \nabla H(P_p) - \sigma_p k_p (P_p - P_t) \tag{5}$$

where σ_t = the solubility of oxygen in muscle tissue, σ_p = the solubility of oxygen in the coronary perfusate, D_t = the coefficient of diffusion of oxygen in muscle tissue, D_p = the coefficient of diffusion of oxygen in the coronary perfusate, D_{Mb} = the coefficient of diffusion of myoglobin in muscle tissue, $\mathbf{u}$ = blood velocity, k_t = coefficient of exchange from perfusate to tissue, k_p = coefficient of exchange from tissue to perfusate, and the (nonlinear) functions F, M, and H relate myoglobin saturation, rate of mitochondrial oxygen consumption, and hemoglobin saturation, respectively, to oxygen partial pressure (see below).

Equations 4 and 5 apply to separate regions of space—namely, muscle tissue and blood vessels, respectively. If the relative volume of the cardiovascular system is denoted by R, then it is appropriate to scale Eqs. 4 and 5 by the factors $(1 - R)$ and R respectively. Oxygen is exchanged between the perfusate and the muscle compartment due to a difference in partial pressure: $(P_p - P_t)$. The exchange coefficients (k_p and k_t) are the proportionality constants of these two fluxes. Because the exchange terms must cancel when the scaled equations are added, it follows that

$$\sigma_p k_p R = \sigma_t k_t (1 - R) \tag{6}$$

(Note that the ratio of solubilities: σ_t/σ_p, is defined by van Beek et al. (1992) as λ, the partition coefficient.)

The model contains two advection terms. One describes the movement of dissolved oxygen as it is transported by the moving blood, whereas the other describes the movement of oxygen bound to hemoglobin within the red blood cell. The four transient terms represent the rates of storage of oxygen dissolved in either the tissues or blood or bound to either myoglobin or hemoglobin. The three diffusion terms describe the rates of change of oxygen partial pressure (in the *negative* gradient direction) due to: the diffusion of unbound oxygen within cardiac muscle, the diffusion of bound oxygen within cardiac muscle (i.e., in the form of oxymyoglobin), and the diffusion of unbound oxygen within the blood. It is assumed that the reversible reaction of oxygen with the transport molecules, myoglobin and hemoglobin, occurs instantaneously.

The three nonlinear functions: F, H, and M (which relate the local or tissue partial pressure of oxygen to oxymyoglobin saturation, oxyhemoglobin saturation and mitochondrial oxygen consumption, respectively) share the same analytical (Michaelis-Menten) description. Each contains two parameters: P_{50} and n. P_{50} is the oxygen partial pressure that yields 50% saturation, in the case of myoglobin and hemoglobin, or 50% activity (commonly signified K_m), in the case of metabolism. The value of the exponent n determines the shape and steepness of the relation. If $n = 1$, then the relation is hyperbolic; if $n > 1$, then the relation is sigmoidal.

$$s(P) = P^n/(P_{50}^n + P^n) \tag{7}$$

In Eq. 7 saturation, or s(P), denotes f, h, or m (myoglobin saturation, hemoglobin saturation, or the relative rate of mitochondrial oxygen consumption, respectively); it is dimensionless and varies between 0 and 1. Each of the relations F, H, and M (Eqs. 4 and 5) is obtained by multiplying its normalized relation (f, h, and m, respectively) by its corresponding scaling parameter: f_{max}, h_{max}, and m_{max}, respectively. The standard values of these (and other parameters) are given in Table 1.

Single-field steady-state model

Equations 4–7 describe a two-field model of oxygen exchange in the heart. In this formulation, the entire complexity of oxygen transport within the coronary vasculature is described by one field (i.e., Eq. 5). Clearly, additional fields (modeling, in detail, the oxygen transport properties of the coronary vascular tree) could be included if warranted. In this initial investigation of the behavior of the *arrested* heart, where perfusion conditions do not vary with time, we focus on a single-field model and its ability to mimic experimentally determined rates of cardiac oxygen consumption under a variety of perfusion conditions.

The single-field model arises when P_p (the oxygen partial pressure of the coronary perfusate) is either a constant or a specified distribution. In this case, Eq. 5 is no longer needed. Substituting the normalized variables f and m into Eq. 4 and rewriting P_a (arterial PO_2) for P_p yields

$$\sigma_t \frac{\partial P_t}{\partial t} + \frac{\partial F(P_t)}{\partial t} - \sigma_t D_t \nabla^2 P_t = \sigma_t k_t (P_a - P_t) + f_{max} D_{Mb} \nabla^2 f(P_t) - m_{max} m(P_t). \tag{8}$$

With this simplification, it is to be understood that oxygen is both supplied to, and consumed at, each point in the tissue. (We show later that the oxygen exchange coefficient k_t must now become dependent on the simulated rate of flow $\dot{V}^s$ into the capillary bed.) Note that Eq. 8 implicitly assigns a value of zero to R, the proportion of heart volume occupied by the coronary vasculature. This assignment mimics the common experimental procedure of normalizing the rate of oxygen consumption per gram of heart tissue.

The second simplification arises by ignoring time-dependent changes in P_t. This is appropriate when considering the measurement of oxygen consumption of the *arrested* heart (Loiselle, 1989). Under this steady-state assumption, rearrangement of Eq. 8 yields

$$\sigma_t k_t (P_t - P_a) = \sigma_t D_t \nabla^2 P_t + f_{max} D_{Mb} \nabla^2 f(P_t) - m_{max} m(P_t). \tag{9}$$

Note that if $f_{max} = 0$ (i.e., if the intramuscular concentration of myoglobin, and hence its contribution to facilitated oxygen diffusion, is ignored)

TABLE 1 Parameters of the model

Parameter	Units	Literature values (at 37°C)								37°C	5°C
σ_t	nmol/mm^3 kPa	0.009924	(12)	0.01013	(16)					0.008035	0.01623
D_t	mm^2/ks	1.5	(12)	1.26–1.5	(16)	2.0	(40)	1.5	(34)	1.5	0.606
σ_p	nmol/mm^3 kPa	0.0117	(12)							0.008829	0.01784
D_p	mm^2/ks									1.5	0.606
k_t	1/ks									107.69*	
D_{Mb}	mm^2/ks	0.03–0.27	(12)	0.027	(39)	0.02–0.027	(16)	0.186	(40)	0.016 (2)	0.07	0.0283
f_{max}	nmol Mb/mm^3	0.28–1.0	(12)	0.45–3.57	(16)	0.28	(40)				0.28	
P_{50} (Mb)	kPa	0.37	(48)	0.48	(55)	0.1	(41)				0.6666	
n (Mb)		1.03	(48)								1	
h_{max}	nmol Hb/mm^3	2.308	(31)								2.3077	
P_{50} (Hb)	kPa										3.333‡	
n (Hb)											2.6‡	
m_{max}	nmol/mm^3 ks	50	(12)	50	(40)	196.85	(54)				10.33	2.822
P_{50} (Mito)	kPa	0.11	(24)	0.1	(59)	0.3	(9)	0.006–0.06	(54)		0.1333	
n (Mito)											1	

Leftmost two columns: parameters and their units; rightmost two columns: parameter values of the model at 37°C and 5°C; middle columns: selected literature values at 37°C (references shown in parentheses). Mb, Hb, Mito: myoglobin, hemoglobin and mitochondrial oxygen consumption, respectively.

* The numeric value of k_t is given, after van Beek et al. (57), by: $2\rho\sigma_p/\sigma_t \times$ flow, where $\rho = 1.05$ g/ml is the specific density of muscle (21) and flow = 2.8 ml/min/g of wet weight (35) is the coronary flow rate.

‡ Calculated, from tabulated data (1) according to Eq. 7. For values at 5°C: σ_p calculated with $Q_{10} = 0.83$ (35); σ_t calculated from σ_p assuming tissue/perfusate solubility ratio to be independent of temperature; D_t from Hill (20); D_{Mb} from Moll (39).

and $m(P_t) = 1$ (i.e., if the rate of oxygen consumption by the mitochondria is assumed to be independent of the oxygen partial pressure), then Eq. 9 becomes equivalent to the single-field description developed by van Beek et al. (1992). In that description, the heart is ascribed a slab geometry and the one-dimensional diffusion equation is solved analytically. Implicit in that model is the assumption that longitudinal PO_2 gradients within the heart wall are negligible.

To test the assumption that longitudinal gradients of PO_2 (and hence diffusion of oxygen in the longitudinal direction) are negligible, we approximated the heart by its left ventricle (LV). We adopted a smooth prolate spheroid geometry and modeled the LV wall and its cavity by two prolate spheroidal halves, one inside the other (see Appendix, Fig. A.1). The nonlinear, steady-state, single-field equation (Eq. 9) was solved for this three-dimensional, axially symmetric geometry using finite element techniques, the details of which are provided in the Appendix. Solution of Eq. 9 yields the PO_2 profile across the heart wall, i.e., in the transmural direction. Comparison of transmural profiles computed for apex and base demonstrates (Fig. A.2) that there is negligible azimuthal variation of PO_2 in the mid-wall region, remote from surface influences. This result confirms the assumption that, at least in the arrested heart, there is negligible longitudinal diffusion of oxygen within the heart wall and justifies simplification of the geometry to a slab model. Further justification is provided by the fact that, over a wide range of parameter values, there was precise agreement of PO_2 values between the slab and prolate spheroidal geometries in the central regions of the wall, remote from the influences of surface flux.

Calculation of oxygen uptake and oxygen consumption

In common experimental practice, the rate of oxygen uptake of the heart is calculated, using the Fick Principle, as the product of perfusate flow and the arteriovenous difference in oxygen content (Eq. 1). It is not possible to determine experimentally the local venous oxygen content because of the natural averaging effect that occurs within the venous system. In the present single-field model the *venous* oxygen content has no meaning; rather it is the local *tissue* oxygen partial pressure (P_t) that is computed. Nevertheless, it is possible to compute the rate of oxygen uptake that would prevail if the Fick Principle were applied to the simulated data ($\dot{V}^s_{O_2}$). In the present formulation, we model hemoglobin-free, saline perfusion that is assumed to be uniformly distributed throughout the tissue. This allows the mean tissue oxygen partial pressure ($\bar{P}_t$) to be calculated as a volume-weighted rather than a flow-weighted average (see Appendix). Hence $\dot{V}^s_{O_2}$, the simulation equivalent of the experimentally determined rate of oxygen uptake, is proportional to the difference in oxygen partial pressure between the arterial supply (P_a) and the mean tissue value ($\bar{P}_t$)

$$\dot{V}^s_{O_2} = \sigma_p \dot{V}^s (P_a - \bar{P}_t). \tag{10}$$

In this formulation, which is the simulation analog of the Fick principle expressed in Eq. 1, $\dot{V}^s$ is the simulated rate of coronary flow. The exchange coefficient k_t (of Eqs. 4, 8, and 9) depends, in some manner yet to be determined (see Results and Discussion), on $\dot{V}^s$.

Mean tissue oxygen partial pressure ($\bar{P}_t$) is calculated by averaging P_t over all elements that constitute the geometric mesh (see Appendix for details). The simulated rate of oxygen consumption ($\bar{m}$) is calculated similarly. The simulated diffusive flux (J) is the difference between the equivalent Fick-expression for oxygen uptake (Eq. 10) and the simulated rate of oxygen consumption

$$J = \dot{V}^s_{O_2} - \bar{m}. \tag{11}$$

Under a variety of conditions, the rate of oxygen uptake simulated according to the Fick principle ($\dot{V}^s_{O_2}$, Eq. 10) was compared with that determined experimentally according to the Fick principle ($\dot{V}^m_{O_2}$, Eq. 1). In these comparisons, no attempt was made to maximise the goodness-of-fit between theoretical and experimental results. For example, a single value of m_{max}, the PO_2-independent rate of mitochondrial oxygen consumption, was employed (at specified temperature) in all simulations despite the fact that the observed rate of resting metabolism varied both between experimental series and among hearts in a given series. Likewise, no attempt was made to simulate the observed variability among hearts in the rate of coronary flow at fixed perfusion pressure.

RESULTS

The behavior of the simplified (i.e., nonlinear, single field, steady state) model of oxygen exchange (Eq. 9) applied to the simplified (i.e., slab) geometry was fully explored by parameter variation. In the present communication we wish to limit attention to several specific issues related to the discrepancy between simulated rates of oxygen consumption ($\bar{m}$) and experimentally measured values of oxygen uptake ($\dot{V}^m_{O_2}$). To do this we use simulation parameter values selected to mimic those that we employed experimentally to measure the rate of oxygen uptake of isolated, Langendorff-circulated, saline-perfused, K^+-arrested, guinea pig hearts.

Simulated tissue PO_2 profiles

Tissue PO_2 (P_t) profiles for a range of environmental PO_2 (P_{env}) values, are shown in Fig. 1. The symmetrical nature of the profiles reflects the identical boundary conditions at the epicardial and endocardial surfaces of the slab. Note the influence of ambient PO_2 extending into the slab to a variable extent depending on the value of P_{env}. For any set of metabolic and perfusion parameters, there is a unique value of P_{env} that renders the P_t profile flat. In the particular case shown in Fig. 1, where P_a is 90.26 kPa, the critical value of P_{env} is 78.34 kPa. When P_{env} is either above or below this value, the mean tissue PO_2 ($\bar{P}_t$) is, respectively, above or below the value of P_t at the center of the slab. It should be noted that if an isolated heart experiment were to be performed using the critical value of P_{env}, then application of the Fick Principle would yield a value of $\dot{V}^m_{O_2}$ uncontaminated by exchange of oxygen between the heart and its environment.

Effect of arterial PO_2 on simulated and experimentally measured rates of oxygen uptake

In Fig. 2 *A* are shown the simulated rate of oxygen uptake ($\dot{V}^s_{O_2}$, see Eq. 10) and the simulated rate of oxygen consumption ($\bar{m}$, see Appendix) together with their difference, the diffusive flux (J, see Eq. 11), computed for a range of values of P_a. For these simulations, P_{env} was set to 20.27 kPa (corresponding to room air). Two behaviors are of note. First, the simulated rate of oxygen consumption ($\bar{m}$) increases steadily with increasing values of arterial oxygen partial pressure up to about 15 kPa. Beyond this point, simulated myocardial metabolism is independent of P_a. This reflects the underlying form of the $m = m(P_t)$ relation, which describes the dependence of mitochondrial oxygen consumption on tissue oxygen partial pressure (Eq. 7). Second, the direction of net oxygen flux (J) across the boundaries depends on the PO_2 gradient between the myocardial tissue and the environment. Net flux is zero when P_{env} equals the average tissue PO_2 ($\bar{P}_t$) which, in this case, is about 30 kPa. That is, for any value of P_{env}, there is a value of P_a above which $\dot{V}^s_{O_2}$ (computed according to the Fick principle) increasingly exceeds the true metabolic rate, $\bar{m}$. With P_{env} = 20.27 kPa (Fig. 2 *A*) the diffusive flux may be positive or negative, depending on the value of P_a.

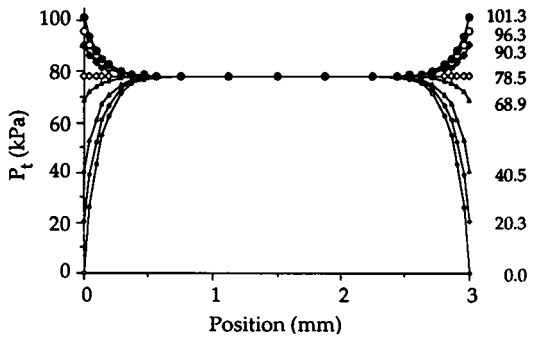

FIGURE 1 Steady-state tissue PO_2 profiles (P_t), computed for slab geometry at the indicated values of P_{env} (kPa); P_a = 90.26 kPa. The slab is 3 mm thick from endocardium (x = 0) to epicardium (x = 3).

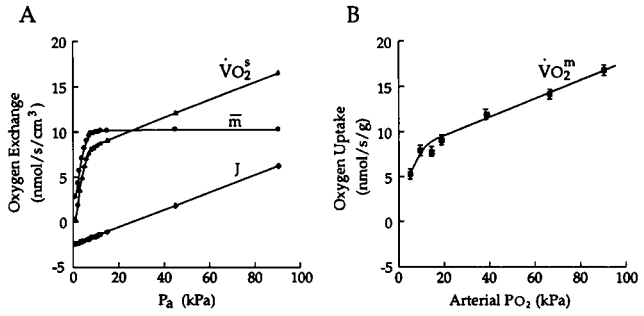

FIGURE 2 Effect of arterial oxygen partial pressure (P_a) on rates of oxygen exchange at 37°C. (*A*) Simulated rate of oxygen uptake computed according to the Fick Principle ($\dot{V}^s_{O_2}$), simulated true rate of oxygen consumption ($\bar{m}$) and their difference (J), the diffusive flux of oxygen across the epicardial and endocardial surfaces; P_{env} = 20.27 kPa. (*B*) Experimentally measured rate of oxygen uptake ($\dot{V}^m_{O_2}$) of 14 K^+-arrested guinea pig hearts; line fitted by eye.

Comparison of Fig. 2 *B* with Fig. 2 *A* shows that the simulated dependence of the rate of oxygen uptake on arterial PO_2 reflects a similar phenomenon observed experimentally. Data arising from experiments on 14 isolated, KCl-arrested guinea pig hearts, perfused with saline equilibrated at 7 different values of arterial PO_2, are presented in Fig. 2 *B*. The hearts were maintained inside a glass chamber that was in communication with room air. As was the case for the simulated data, dependence of the experimentally measured rate of oxygen uptake on P_a is evident, including its more-or-less linear nature above a value of some 15 to 20 kPa. The ability of the theoretical model (Fig. 2 *A*) to mimic the experimental results (Fig. 2 *B*), without recourse to parameter optimization, is striking.

Effect of environmental PO_2 on simulated and experimentally measured rates of oxygen uptake

The environmental partial pressure of oxygen (P_{env}) has an effect on the simulated rate of oxygen uptake ($\dot{V}^s_{O_2}$) at any value of arterial oxygen partial pressure (P_a). The effect is greater the larger the difference between P_a and P_{env} and is accentuated by a low metabolic rate (m_{max}). In fact, if the values of both P_a and m_{max} are low, then $\dot{V}^s_{O_2}$ can even become negative for large values of P_{env} (Fig. 3 *A*). For an arterial oxygen partial pressure of 19.01 kPa (corresponding to equilibration with 20% O_2), and the set of simulation parameters given in the right-most column of Table 1, $\dot{V}^s_{O_2}$ becomes negative for values of P_{env} in excess of about 50 kPa. Note that the simulated rates of oxygen consumption and oxygen uptake coincide when $P_{env} \approx P_a$, reflecting the low value of m_{max} used in this simulation.

Similar behavior is observed experimentally. Fig. 3 *B* shows the results of an experiment in which five guinea pig hearts were perfused with oxygenated saline, equilibrated with 20% O_2 at 5°C, while the ambient PO_2 was varied from 0 to 90 kPa. In this experiment the mean content of oxygen in the venous effluent exceeded that in the

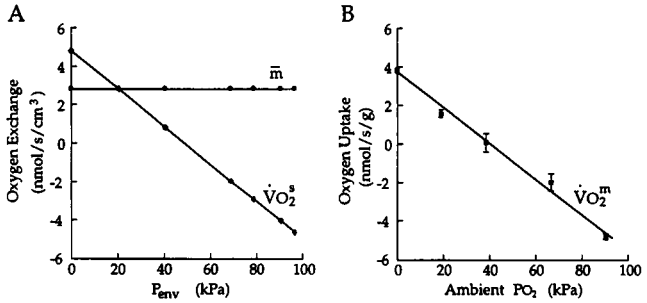

FIGURE 3 Effect of environmental oxygen partial pressure (P_{env}) on (*A*) simulated and (*B*) experimentally measured, $n = 5$, rates of oxygen uptake at 5°C. Symbols have the same meanings as in Fig. 2.

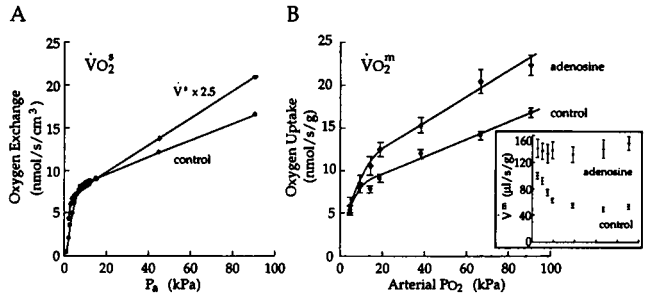

FIGURE 4 Effect of coronary flow on oxygen exchange-arterial PO_2 relations. (*A*) Simulated effect of a 2.5-fold increase of flow ($\dot{V}^s$); $P_{env} = 20.27$ kPa. (*B*) Experimental results from 14 control hearts (same data as in Fig. 2 *B*) and from 14 different hearts suspended in room air and perfused with 2 mM adenosine at constant perfusion pressure. (*Inset*) Coronary flow ($\dot{V}^m$) as a function of arterial PO_2.

arterial perfusate for all values of P_{env} in excess of about 40 kPa. Once again, and with no attempt to optimize parameters, the simulated results (Fig. 3 *A*) closely model those measured experimentally (Fig. 3 *B*).

Effect of coronary flow on simulated and experimentally measured rates of oxygen uptake

Under the classical Fick principle (Eq. 1), any change of coronary flow, $\dot{V}^m$, at constant metabolic rate would induce an inverse change in the arteriovenous difference of oxygen content such that $\dot{V}^m_{O_2}$ would remain constant. The theoretical model is more robust in this regard and is not subject to this constraint. The simulated rate of oxygen uptake ($\dot{V}^s_{O_2}$, Eq. 10) requires calculating the product of simulated coronary flow ($\dot{V}^s$) and the difference between P_a and $\bar{P}_t$, the computed mean tissue PO_2. As has been demonstrated above, the latter value may be influenced directly by P_{env}. But it is also possible that it is influenced indirectly by variation of the exchange coefficient k_t—through some dependence of that parameter on $\dot{V}^s$. As a first step toward testing this notion, k_t was assumed to be directly proportional to $\dot{V}^s$ and simulations were performed to see if the simulated rate of oxygen uptake, $\dot{V}^s_{O_2}$, is sensitive to $\dot{V}^s$.

The results are shown in Fig. 4 *A* for $P_{env} = 20.3$ kPa. For all values of P_a above about 15 kPa, the simulated 2.5-fold increase of coronary flow leads to a larger value of $\dot{V}^s_{O_2}$ than that computed for "control" conditions. Below this "critical" value of P_a, the behavior of $\dot{V}^s_{O_2}$ becomes more complicated and P_{env}-dependent. If $P_{env} = 0$ kPa, then the two $\dot{V}^s_{O_2}$ curves do not intersect, reflecting the fact that J, the flux of O_2 from tissues to surrounds, is always positive in this situation.

Once again, comparable results obtained under experimental conditions. Fig. 4 *B* summarizes the results of an experimental series in which the rate of oxygen uptake of 14 KCl-arrested guinea pig hearts was measured in the presence of the coronary vasodilator adenosine (2 mM). For convenience, the corresponding data for the control group of 14 hearts, recorded in the absence of adenosine, are re-plotted from Fig. 2 *B*. As can be seen in the inset of Fig. 4 *B*, the rate of coronary flow in the adenosine-treated group was independent of arterial PO_2 and averaged 138 $\mu l\ s^{-1}\ g^{-1}$. Control hearts, on the other hand, spontaneously vasodilated under conditions of low arterial PO_2 (20 kPa or less) but remained vasoconstricted at higher values of PO_2. In the latter region, the average rate of coronary flow under control conditions was 52.4 $\mu l\ s^{-1}\ g^{-1}$. Hence adenosine effected a 2.6-fold increment of measured coronary flow comparable to the 2.5-fold increment simulated in Fig. 4 *A*. Better agreement of oxygen uptake values between theory (Fig. 4 *A*) and experiment (Fig. 4 *B*) could probably have been obtained by using a more accurate description of the relationship between $\dot{V}^s$ and k_t (than the direct proportionality assumed here), but no attempt was made to explore this possibility.

These results demonstrate that variation of coronary flow can distort experimental estimates of the rate of myocardial oxygen consumption made using the Fick principle. However, the design of the experiment made it difficult to isolate the effect of flow per se, because arterial PO_2 itself modulates coronary vascular resistance (see inset of Fig. 4 *B* where it is evident that vasodilation occurred at low values of arterial PO_2). To avoid this problem, a separate set of experiments was performed in which coronary flow was varied by changing coronary perfusion pressure at a constant arterial PO_2 of 90 kPa.

In this experimental series, seven KCl-arrested guinea pig hearts were subjected to seven different values of coronary perfusion pressure (2.67–19.67 kPa) in the usual Latin Square design. Environmental PO_2 was held constant at either 0 or 90 kPa. Because perfusion pressure was the independent variable, standard error bars accompany the measured values of coronary flow rate shown in Fig. 5 *B*. It is clear that the measured rate of oxygen uptake, calculated according to the Fick principle, was greater at the lower value of environmental PO_2. Furthermore, despite a considerable amount of scatter in the data, it is likewise clear that the experimentally measured rate of oxygen consumption depends on the rate of coronary perfusion. It is of considerable importance to know how much of this observed dependence is attributable to the diffusive exchange of oxygen from tissues to environment and how much reflects a true flow-dependence of cardiac resting metabolism. To that end, simulations were performed in which the value of $\dot{V}^s$ was varied

over a wide range while m_{max}, the simulated maximal rate of oxygen consumption, was held constant at a value of 10.3 nmol s^{-1} cm^{-3}.

The results of these simulations are presented in Fig. 5 *A*. Consider, first, the inset that shows the variation of the true rate of myocardial oxygen consumption ($\bar{m}$) with coronary flow ($\dot{V}^s$) for both a high and a low value of P_{env}. These relations reflect the underlying $m = m(P_t)$ relation (Eq. 7). That is, when the rate of coronary flow decreases sufficiently, then $\bar{P}_t$ eventually falls to the left of the "shoulder" of the hyperbolic $m = m(P_t)$ relation, and the rate of oxygen consumption becomes compromised. The extent to which this occurs depends on the gradient that drives diffusive oxygen exchange between the tissues and their surrounds. When P_{env} = 90.3 kPa and thus exceeds $\bar{P}_t$ (upper curve, *inset*), then the simulated oxygen consumption-flow relation lies above that computed for the case when P_{env} = 0 kPa. In the former condition, the rate of oxygen consumption in the surface regions of the slab is enhanced by the diffusive supply of oxygen from the environment. But once the simulated rate of flow exceeds about 10 μl s^{-1} cm^{-3}, then the rate of oxygen consumption is essentially maximal.

The graph of simulated oxygen uptake ($\dot{V}^s_{O_2}$, Fig. 5 *A*), by contrast, fails to reach a maximum when P_{env} is zero. Although the simulated rate of oxygen consumption saturates (*inset*), the rate of oxygen uptake fails to reach a plateau even if the rate of coronary flow is increased to unphysiologically high values. In this condition, J (the flux of oxygen from tissue to surrounds) can become very large relative to $\bar{m}$. The situation is only marginally better when P_{env} is 20.3 kPa (corresponding to room air). Contrarily, when P_{env} is 90.3 kPa (and therefore exceeds $\bar{P}_t$), $\dot{V}^s_{O_2}$ underestimates $\bar{m}$ at all rates of flow. These simulation results (Fig. 5 *A*) are in qualitative agreement with the corresponding experimental results (Fig. 5 *B*), although the quantitative agreement is poorer than for any of the preceding comparisons (Figs. 2–4).

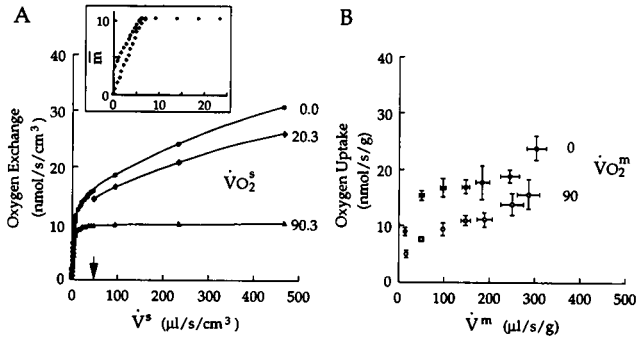

FIGURE 5 Effect of coronary flow on oxygen exchange. (*A*) Simulated rate of oxygen uptake, $\dot{V}^s_{O_2}$, computed for the three values of P_{env} indicated, as a function of flow, $\dot{V}^s$, with m_{max} = 10.33 nmol s^{-1} cm^{-3}. (*Arrow*) Standard flow simulation value (46.7 μl s^{-1} cm^{-3} ≡ 2.8 ml min^{-1} g^{-1} ≡ 107.69 ks^{-1}, see Table 1). (*Inset*) Simulated rate of mitochondrial oxygen consumption, $\bar{m}$, as a function of flow for P_{env} of 90.3 kPa (*open symbols, upper curve*) and 0 kPa (*closed symbols, lower curve*). (*B*) Experimentally measured rates of oxygen uptake, $\dot{V}^m_{O_2}$, as a function of coronary flow ($\dot{V}^m$), of seven K^+-arrested guinea pig hearts; arterial PO_2 = 90 kPa. Ambient PO_2 was either 0 kPa (*closed symbols*) or 90 kPa (*open symbols*). Coronary flow varied by varying perfusion pressure; SE bars are occasionally smaller than symbols.

DISCUSSION

Two papers, published early this century, have dominated thinking about oxygen supply to tissues. Hill (1928), utilizing Carslaw's (1921) extensive treatment of heat conduction in solids, provided a thorough analysis of oxygen supply to isolated, unperfused tissues. Supply was purely by diffusive means, and tissues were constrained to have simple geometric shapes in order to allow analytical solutions of the diffusion equation. Earlier Krogh (1919) had provided an analysis, based on similarly idealized geometry, of advective oxygen supply, via a central cylindrical capillary, combined with diffusive exchange between the capillary and a concentric annulus of tissue. No exchange between adjacent capillary units was admitted. These models have been extensively applied, critically examined (Kreuzer, 1982; Piiper and Scheid, 1986), and variously extended (Groebe, 1990; Honig et al., 1984; Lagerlund and Low, 1987; Mainwood and Rakusan, 1982; Popel and Gross, 1979). In particular, numerous authors have incorporated myoblobin-facilitated diffusion of oxygen (Baylor and Pape, 1988; de Koning et al., 1981; Fletcher, 1980; Gonzalez-Fernandez and Atta, 1982; Kreuzer and Hoofd, 1984; Loiselle, 1987; Murray, 1974; Salathé and Kolkka, 1986; Stroeve, 1982), the kinetics of oxygen-hemoglobin (Brittain and Simpson, 1989; Clark et al., 1985), or oxygen-myoglobin (van Ouwerkerk, 1977) interaction and the dependence of mitochondrial oxygen consumption on oxygen partial pressure (de Koning et al., 1980; Loiselle, 1982; Taylor and Murray, 1977). In addition, diffusion shunting of oxygen between adjacent capillaries (Grunewald and Sowa, 1978) or between distribution and drainage vessels (Piiper et al., 1984) has been considered. A model of a thin region of tissue, proximal to the surface of an organ, in which oxygen is supplied by diffusion simultaneously from both the environment and from capillaries has been developed by Popel and colleagues (Klitzman et al., 1983; Popel, 1981), but is not well suited to model the thick wall of the heart.

The two-field model developed in the current study incorporates most of the features just enumerated: advection, simple diffusion, facilitated diffusion, PO_2 dependence of metabolic rate, and diffusive exchange both within the tissue per se and between tissue and external surrounds. In the most general form of the model, advection is confined to a vascular compartment of relative magnitude R. The model assumes the following conditions. (i) Oxygen solubility (σ) varies among media but has no spatial dependence within a medium. (ii) Oxygen diffusivity (D) is isotropic and spatially homogeneous. (iii) The diffusion of oxygen is facilitated by the presence of myoglobin; the kinetics of oxymyoglobin interaction are instantaneous. (iv) The rate of oxygen consumption varies with the local tissue PO_2. (v) When simplified to a single field, the perfusate is assumed to be saline

that is uniformly distributed throughout the tissue. (vi) Attention is confined to the steady-state in order to simulate oxygen exchange during cardiac arrest.

The constants k_t and k_p (see Eq. 6) ensure coupling between the two advection-diffusion equations (i.e., between Eqs. 4 and 5). Upon reduction to a single-field description (Eq. 9), k_t (which has dimensions of $time^{-1}$) becomes dependent upon the rate of coronary flow ($\dot{V}^s$). The physical mechanism underlying this dependence is unknown, but it may be speculated that an increase of coronary flow results in the perfusion of a greater proportion of the capillary bed, whereas any increase of coronary pressure leads to a distension of the coronary capillaries (Schouten et al., 1992). Capillary distension would increase the surface area for diffusive exchange while simultaneously decreasing the effectiveness of any diffusion barrier offered by the capillary endothelium. Under a given set of perfusion conditions, any or all of these mechanisms (capillary recruitment, increased surface area, or decreased diffusion distance) could contribute to the dependence of advective-diffusive coupling on coronary flow.

It would be a straightforward matter to extend the model to include as many distinct fields (to reflect the properties of separate divisions of the coronary vascular circuit) as may be required to model any observed oxygen transport phenomenon. An important conclusion of the current investigation is that a single-field approximation satisfactorily simulates a wide range of experimental observations made at the macroscopic level in the arrested heart (see also van Beek et al. (1992)). These observations support earlier claims (Follert, 1971; Loiselle, 1989; Loock and Schmidt,1986) that the surface of the isolated heart is freely permeable to oxygen. In consequence, oxygen is lost from the myocardium to its surrounds whenever the environmental partial pressure of oxygen (P_{env}) is lower than the mean tissue partial pressure of oxygen ($\bar{P}_t$), which itself is a function of the prevailing arterial oxygen partial pressure (P_a), rate of coronary flow ($\dot{V}$), and the PO_2-independent metabolic rate (m_{max}). Conversely, oxygen will be gained by the myocardium whenever the transmural gradient is reversed.

Influence of arterial PO_2 (P_a)

The diffusive exchange of oxygen between the isolated heart and its surrounds is driven by the difference in partial pressure between tissue and environment ($\bar{P}_t - P_{env}$). Because $\bar{P}_t$ depends on the prevailing arterial oxygen partial pressure (P_a), some dependence of $\dot{V}^m_{O_2}$, the experimentally measured rate of oxygen consumption of the heart, on P_a is to be expected—even in a PO_2 range where m, the rate of mitochondrial oxygen consumption, is maximal. This expectation was supported by both simulation and experimental observation. At low values of P_a, both the simulated (Fig. 2 *A*) and the experimentally observed (Fig. 2 *B*) rates of oxygen consumption fall, reflecting the underlying nonlinear dependence of mitochondrial metabolism on tissue oxygen partial pressure ($m = m(P_t)$, Eq. 7). (Note that this behavior would not be anticipated by any model in which the rate of mitochondrial oxygen consumption is independent of oxygen partial pressure.) At high values of P_a, both $\dot{V}^s_{O_2}$ and $\dot{V}^m_{O_2}$ increasingly diverge from the true rate of oxygen consumption. The linear nature of this divergence can be attributed to saturation of the $m = m(P_t)$ relation such that P_{env} makes a negligible further contribution. What had previously been misinterpreted as a nonsaturating dependence of cardiac oxygen consumption on coronary oxygen supply (Kenwright and Loiselle, 1986) is now revealed as a consequence of the diffusive flux of oxygen from tissue to environment whenever the average tissue partial pressure of oxygen exceeds the ambient PO_2.

Influence of environmental PO_2 (P_{env})

If the oxygen partial pressure of the surrounds (P_{env}) becomes sufficiently large with respect to P_a, then the measured rate of oxygen consumption can become negative. This behavior, the effect of which is exacerbated by a low metabolic rate, was first reported by Loiselle (1989) and the data are re-presented here as Fig. 3 *B*. In those experiments the arterial PO_2 was 20 kPa, and perfusion temperature was lowered to 5°C in order to reduce the metabolic rate. The observed rate of oxygen consumption became negative at values of P_{env} above about 40 kPa (Fig. 3 *B*), reflecting net flux of oxygen into the heart from the environment. The mathematical model shows similar behavior of the simulated rate of oxygen consumption (Fig. 3 *A*); $\dot{V}^s_{O_2}$ becomes negative for all values of P_{env} in excess of about 50 kPa. It is of interest that the simulated true rate of oxygen consumption, $\bar{m}$, is essentially independent of P_{env} under these conditions (Fig. 3 *A*). This behavior reflects the much reduced value of m_{max} and the considerably higher value of oxygen solubility at 5°C *vis a vis* 37°C (see Table 1) such that tissue PO_2 remains on the plateau of the $m = m(P_t)$ relation throughout the extent of the slab. The independence of $\bar{m}$ from the influence of P_{env} under these simulation conditions assures that the variation of $\dot{V}^s_{O_2}$ with P_{env} is linear throughout its entire range.

Influence of rate of flow of coronary perfusate ($\dot{V}^s$)

The earlier algebraic model of Loiselle (1989) implicitly disallowed any dependence of $\dot{V}^s_{O_2}$ on the rate of coronary flow. By contrast, the current model, like the analytical one of van Beek et al. (1992), clearly shows a dependence of the measured rate of oxygen uptake on coronary flow. In Fig. 4 *A*, a 2.5-fold increase of flow is seen to exacerbate the arterial PO_2-dependent overestimation of $\bar{m}$ at all but the lowest values of P_a. This behavior of the slab model mimics that observed in the arrested whole heart (Fig. 4 *B*). When coronary flow is increased, via adenosine-induced vasodilation under constant perfusion pressure, the rate of resting oxygen consumption apparently increases. That this increase is artefactual, and attributable to the diffusive loss of oxygen from the

heart to its surrounds, is supported by the evidence presented in Fig. 5 *B* from experiments conducted at variable perfusion pressure.

Under the assumption that perfusion pressure has no effect on m_{max} (the PO_2-independent, maximal metabolic rate), the simulated rate of oxygen uptake nevertheless depends on flow (Fig. 5 *A*). This dependence itself varies with environmental PO_2; the lower the value of P_{env} the greater the discrepancy between $\dot{V}^{s}_{O_2}$ and $\bar{m}$ for any flow rate. Even when the environmental PO_2 is 20 kPa (corresponding to room air), the effect of flow on $\dot{V}^{s}_{O_2}$ is so large as to render the latter quantity essentially useless as an estimator of $\bar{m}$ (at least when $P_a = 90$ kPa). A comparable (albeit linear) dependence of the rate of oxygen uptake on coronary flow in isolated, KCl-arrested, guinea pig hearts suspended in room air was reported by Follert (1971). Oxygen uptake, calculated according to the Fick principle, was observed to vary about 7-fold for a 14-fold change of flow. Follert (1971) explicitly recognized this dependence to be artefactual and due to diffusive loss of oxygen from cardiac tissue to the environment.

The effect of environmental PO_2 on the oxygen uptake-flow relation under experimental conditions is exemplified by the data of Fig. 5 *B*. Despite a considerable amount of scatter in these data, the general correspondence with the simulation data of Fig. 5 *A* is clear. Particularly convincing is the upward shift of the relation with a reduction of environmental PO_2 and its dependence on flow. Several other authors have reported a positive correlation between the rate of coronary flow (or perfusion pressure) and the rate of oxygen consumption of isolated, arrested hearts. The data of Lochner, Arnold and Müller-Ruchholtz (Lochner et al., 1968), relating to KCl-arrested guinea pig hearts (see their Table 1), yields a curvilinear relation that is similar to those of Fig. 5. This result has frequently been attributed to a stretch or "garden hose" effect in which increased perfusion pressure passively stretches cardiac muscle cells, thereby increasing their basal metabolic rate. The simulation results of Fig. 5 *A* now make it appear likely that this result reflects, primarily, flow-dependent loss of oxygen from the arterial perfusate (95% O_2-equilibrated) to the environment. A stretch effect at very high perfusion pressures remains a possibility, nevertheless, as indicated by the rightmost data points of Fig. 5 *B*.

Gibbs and Kotsanas (1986) exploited the natural variation of coronary flow rate among different preparations to construct a family of oxygen consumption versus flow relations for isolated rabbit hearts. The hearts had been perfused with a variety of solutions, including some that contained erythrocytes. Arrest was achieved either by lowering Ca^{2+} concentration or by raising K^+ concentration. In every case, the rate of resting oxygen uptake was correlated significantly with the rate of coronary flow. Their data also clearly show the effect of reducing arterial oxygen fraction from 95% to 50%: a parallel downward shift of the oxygen consumption-flow relation. These results are consistent with our interpretation of arterial PO_2-dependent loss of oxygen from the myocardium to the environment with a consequent increase in the *apparent* rate of oxygen consumption (i.e., in the rate of oxygen uptake). Given our simulation results, however, we conclude that the use of *linear* regression to establish oxygen consumption-flow relationships is inappropriate. Hence, no meaning should be attached to the (linearly extrapolated) intercept of a $\dot{V}^{m}_{O_2}$-flow relation. In particular, such an intercept cannot yield an estimate of the diffusion-supplied extent of resting oxygen consumption. The superficial surfaces of both the endocardium and the epicardium can be adequately supplied by diffusion if the environmental PO_2 is high (see Fig. 5 *A*, *inset*, and van Beek et al. (1992)), but the resulting oxygen consumption cannot be measured by any variation of the Fick Principle.

The apparent flow-dependence of cardiac oxygen consumption also obtains if coronary perfusion is manipulated by pharmacological means. When vasodilation is achieved by use of adenosine, under conditions of constant perfusion pressure, then the observed rate of oxygen consumption is increased (Fig. 4 *B*). A similar observation, at a single value of arterial PO_2, has been reported for isovolumically contracting guinea pig hearts using the vasodilatory agent dipyridamole (Gorman et al., 1989). At constant perfusion pressure, dipyridamole increased coronary flow from 88 to 165 $\mu l \cdot s \cdot g^{-1}$ while effecting a 38% increase in the rate of oxygen consumption calculated according to the Fick principle. Given that these hearts were perfused with 95% O_2 and, presumably, suspended in room air, the similarity of this result to those simulated in Fig. 5 *A* is striking. Our results (Figs. 4 and 5) imply that in order to reveal the *direct* effect of a coronary vasodilator on cardiac oxygen consumption, it is more appropriate to perform experiments under conditions of constant coronary flow (Burkhoff et al., 1990; Buxton et al., 1992).

CONCLUSIONS

The above mathematical model of oxygen transport mimics a variety of experimental observations sufficiently well to give confidence that it adequately describes the exchange of oxygen in the heart. By incorporating diffusive as well as advective components, it recognizes various experimentalists' claims of diffusive loss of oxygen directly from arterial supply vessels to coronary capillaries and cardiac tissue (Duling and Berne, 1970; Ellsworth and Pittman, 1990; Popel and Gross, 1979; Popel et al. 1989; Swain and Pittman, 1989; Tateishi et al., 1992). Indeed, the model assumes homogeneous oxygen diffusivity both within myocardial tissue and across its epicardial and endocardial surfaces. Viewed in retrospect, it is curious that diffusive gaseous exchange across surface membranes (recognized as essential for the oxidative support of any isolated, unperfused tissue preparation) has not received more attention from cardiac physiologists. The avascular nature of the teleost heart is well known in the zoological literature (Tota et al., 1983); presumably teleost cardiac muscle receives its supply of oxygen exclusively by diffusion from the ventricular lumen. Such diffusion commonly

operates in reverse in isolated saline-perfused hearts. It provides the source of arterial PO_2-dependent, environmental PO_2-dependent, and coronary flow-dependent errors in the measurement of myocardial oxygen consumption using the classical Fick principle.

APPENDIX 1

The assumption of negligible longitudinal diffusion within the heart wall is examined here using a three-dimensional model based on prolate spheroidal coordinates (Fig. A.1 *A*). During Langendorff perfusion, the right ventricle is filled with coronary venous effluent, whereas the left ventricle (LV) is empty and is commonly either vented (in studies of the beating heart) or aspirated (in studies of the arrested heart). In the latter case the PO_2 boundary conditions may be considered equal at the endocardial and epicardial surfaces. For this reason, and because left ventricular tissue represents the bulk of heart mass, the heart was approximated by its left ventricle.

PROLATE SPHEROIDAL GEOMETRY

The LV cavity and wall are modeled by two prolate spheroid halves, one inside the other (Fig. A.1 *B*). The volume of the cavity is given by $V = 2\pi ab^2/3$. Determination of a, the depth of the left ventricle, and V, the volume of the LV cavity, allows calculation of b, the radius of the LV at its base. A series of measurements was made (Mawson, 1991) on the hearts (mean wet weight 1.25 ± 0.095 g) of five guinea pigs to determine mean parameter values. From measurements made on the silicone rubber cast of a ventricle, a value of 11.5 mm was adopted for a, the depth of the left ventricle. Left ventricular volume, determined by displacement of water by the cast, was approximately 2 ml, from which a value of 2.8 mm was calculated for b, the radius of the inner prolate spheroid shell at the base. By using this value of b, and the expressions for converting between rectangular and prolate spheroidal coordinate systems (given in the legend of Fig. A.1), the geometric equivalent of the guinea pig heart shown in Fig. A.1 *C* was derived.

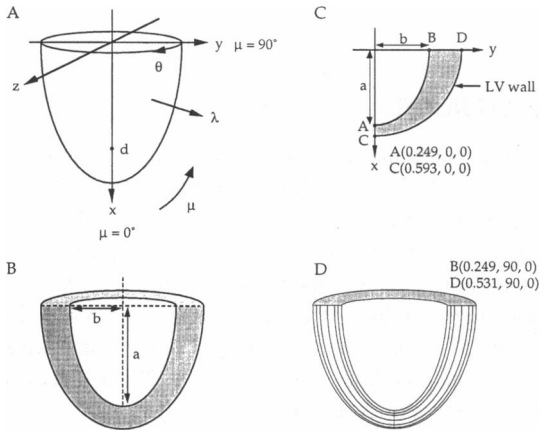

FIGURE A1 The prolate spheroidal approximation of the left ventricle of the guinea pig heart. (*A*) The rectangular and prolate spheroid coordinate systems. Conversion between systems is achieved by: $x = d \cosh \lambda \cos \mu$, $y = d \sinh \lambda \sin \mu \cos \theta$, and $z = d \sinh \lambda \sin \mu \sin \theta$, where d is the focus of the spheroid and λ, μ, and θ describe the transmural, azimuthal, and circumferential directions, respectively. (*B*) The two prolate spheroid shells that define the epicardial and endocardial surfaces of the left ventricle. (*C*) Transmural section of LV wall and cavity that defines the prolate spheroid geometry of the guinea pig left ventricle as employed in the model; coordinates: (λ, μ, θ). (*D*) Axisymmetric prolate spheroid geometry (subdivided by a six-element mesh) used in the finite element analysis procedure. Note the difference in wall thickness between the apex and the base and greater density of elements in the surface regions.

THE FINITE ELEMENT METHOD

The region between the prolate spheroidal shells, which corresponds to left ventricular and septal musculature, is divided into a number of elements bounded by nodes (Fig. A.1 *D*). The number of elements (or nodes) defines the degree of refinement of the geometric "mesh". Solution of Eq. 9 yields the profile of tissue oxygen partial pressure (P_t) as a function of transmural location.

Initially each prolate coordinate (λ, μ, θ) was interpolated linearly. It was necessary to increase the refinement of the mesh considerably (from 5 to 33 nodes) in order to reduce oscillation, in the surface regions, of the solution to Eq. 9 (i.e., the transmural PO_2 gradient). These oscillations are due to the large gradients that occur near the surface that render it impossible for a small number of nodes to interpolate accurately the solution across the extent of the wall. Even with preferential refinement in the surface regions (note the greater density of elements near the surface in Fig. A.1 *D*), a large number of nodes was still required to obtain a satisfactory transmural solution. Refinement in either the azimuthal or circumferential direction was of minimal assistance. The cost involved in such a degree of refinement is an increase in computation time required to achieve a stable solution.

In order to reduce computation time, the basis function used to interpolate the dependent variable in the transmural (λ) direction was changed from linear to cubic Hermite. The cubic Hermite basis function incorporates both the nodal value and its derivative, thereby reducing the number of nodes required to obtain the same degree of accuracy. Figure A.2 shows a number of P_t profiles, for a selection of boundary conditions and P_a = 64.66 kPa, computed using a 6-node mesh. Oscillations that occur in the transmural direction, which are accentuated by the use of cubic Hermite interpolation and are minimal at the apex where wall thickness is least, have been reduced to an acceptable level by increasing the degree of refinement in the endocardial and epicardial regions where the PO_2 gradients are steepest. Comparison between base and apex (Fig. A.2), shows that there is negligible azimuthal variation of PO_2 in the mid-wall region, remote from surface influences.

CALCULATION OF SIMULATED VALUES OF TISSUE PO_2 AND OXYGEN CONSUMPTION

The mean transmural tissue PO_2, averaged over the thickness (L) of the ventricular wall is given by

$$\bar{P}_t = \sum_{e=1}^{E} \bar{P}_e \cdot \Delta l_e \Big/ \sum_{e=1}^{E} \Delta l_e \qquad \text{(A1)}$$

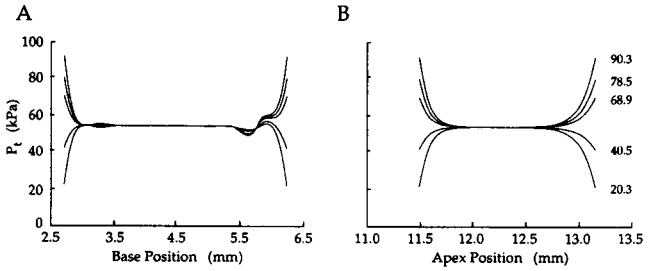

FIGURE A2 Steady-state tissue PO_2 (P_t) profiles, computed using a six-node mesh and cubic Hermite interpolation in the transmural direction, at the (*A*) base and (*B*) apex of the prolate spheroid model for the values of P_{env} (kPa) indicated; P_a = 64.66 kPa. In each panel, the endocardial surface is located at the left and the epicardial surface at the right.

where $\bar{P}_e$ is the average tissue PO_2 within an element of width Δl_e, and the summation is over all E elements that constitute the geometric mesh across L. The average tissue PO_2 within an element ($\bar{P}_e$) is calculated using the local coordinate ξ

$$\bar{P}_e = \int_0^1 P(\xi)\, d\xi \Big/ \int_0^1 d\xi. \quad \text{(A2)}$$

By analogy, the simulated rate of oxygen consumption ($\bar{m}$), uncontaminated by diffusive flux across the epicardial and endocardial surfaces, is calculated by averaging the elemental rates of oxygen consumption ($\bar{m}_e$).

We wish to acknowledge the contributions of Ms. Robyn Lee-Joe and Mr. Stephen Mansell, who explored the consequences of an early mathematical model of oxygen transport in the heart as their final year projects for the Bachelor of Engineering degree. It is a pleasure to thank Patricia Cooper for preparation of the figures.This work was supported by a Project Grant from the National Heart Foundation of New Zealand.

REFERENCES

Altman, P. L., and D. S. Dittmer. 1971. Biological Handbook: Respiration and Circulation. *FASEB J.* 204.

Baylor, S. M., and P. C. Pape. 1988. Measurement of myoglobin diffusivity in the myoplasm of frog skeletal muscle fibres. *J. Physiol.* 406:247–275.

Brittain, T., and R. Simpson. 1989. An analysis of the stopped-flow kinetics of gaseous ligand uptake and release by adult mouse erythrocytes. *Biochem. J.* 260:171–176.

Burkhoff, D., R. Kalil-Filho, and G. Gerstenblith. 1990. Oxygen consumption is less in rat hearts arrested by low calcium than by high potassium at fixed flow. *Am. J. Physiol.* 259:H1142–H1147.

Buxton, D. B., K. Kjaer-Pederson, and A. Nguyen. 1992. Metabolic effects of adenosine in the isolated perfused rat heart. *J. Mol. Cell Cardiol.* 24:173–181.

Carslaw, H. S. 1921. Introduction to the Mathematical Theory of the Conduction of Heat in Solids. Macmillan Publishing Co. Ltd., London.

Clark, A., Jr., W. J. Federspiel, P. A. A. Clark, and G. R. Cokelet. 1985. Oxygen delivery from red cells. *Biophys. J.* 47:171–181.

de Koning, J., L. J. Hoofd, and P. M. Breepoel. 1980. Facilitation of oxygen diffusion in hemoglobin solutions: influence of various salt concentrations. *Adv. Physiol. Sci.* 25:323–324.

de Koning, J., L. J. C. Hoofd, and F. Kreuzer. 1981. Oxygen transport and the function of myoglobin: theoretical model and experiments in chicken gizzard smooth muscle. *Pflügers Arch.* 389:211–217.

Duling, B. R., and R. M. Berne. 1970. Longitudinal gradients in periarteriolar oxygen tension. *Circ. Res.* 27:669–678.

Ellsworth, M. L., and R. N. Pittman. 1990. Arterioles supply oxygen to capillaries by diffusion as well as by convection. *Am. J. Physiol.* 258: H1240–H1243.

Fletcher, J. E. 1980. On facilitated oxygen diffusion in muscle tissues. *Biophys. J.* 29:437–458.

Follert, E. K. 1971. Significance of diffusion loss of oxygen in determining respiration of isolated, perfused organs. *Pflügers Arch.* 323:80–85.

Forster, R. E. 1964. Diffusion of gases. *In* Handbook of Physiology, Respiration. American Physiological Society, Washington, D. C. 839–872.

Gibbs, C. L., and G. Kotsanas. 1986. Factors regulating basal metabolism of the isolated perfused rabbit heart. *Am. J. Physiol.* 250:H998–H1007.

Gonzalez-Fernandez, J. M., and S. E. Atta. 1982. Facilitated transport of oxygen in the presence of membranes in the diffusion path. *Biophys. J.* 38:133–141.

Gorman, M. W., R. D. Wangler, and H. V. Sparks. 1989. Distribution of perfusate flow during vasodilation in isolated guinea pig heart. *Am. J. Physiol.* 256:H297–H301.

Groebe, K. 1990. A versatile model of steady state O_2 supply to tissue: Application to skeletal muscle. *Biophys. J.* 57:485–498.

Grunewald, W. A., and W. Sowa. 1978. Distribution of the myocardial tissue PO_2 in the rat and the inhomogeneity of the coronary bed. *Pflügers Arch.* 374:57–66.

Hill, A. V. 1928. The diffusion of oxygen and lactic acid through tissues. *Proc. Royal Soc.* B104:39–96.

Hill, A. V. 1965. Trails and Trials in Physiology. Edward Arnold Ltd., London. 245 pp.

Honig, J. R., T. E. J. Gayeski, W. Federspiel, A. Clark Jr., and P. Clark. 1984. Muscle O_2 gradients from hemoglobin to cytochrome: new concepts, new complexities. *Adv. Exp. Med. Biol.* 169:23–38.

Hunter, P. J., and B. H. Smaill. 1988. The analysis of cardiac function: A continuum approach. *Prog. Biophys. Molec. Biol.* 52:101–164.

Jöbsis, F. F. 1972. Oxidative metabolism at low PO_2. *Fed. Proc.* 31: 1404–1413.

Kenwright, D. N., and D. S. Loiselle. 1986. Oxygen supply limits basal metabolism in saline-perfused hearts. *J. Mol. Cell Cardiol.* (18, Pt. 1): 299P.

Klitzman, B., A. S. Popel, and B. R. Duling. 1983. Oxygen transport in resting and contracting hamster cremaster muscles: experimental and theoretical microvascular studies. *Microvasc. Res.* 25:108–131.

Kreuzer, F. 1982. Oxygen supply to tissues: the Krogh model and its assumptions. *Experientia.* 38:1415–1426.

Kreuzer, F., and L. Hoofd. 1984. Facilitated diffusion of oxygen: possible significance in blood and muscle. *Adv. Exp. Med. Biol.* 169:3–21.

Krogh, A. 1919. The number and distribution of capillaries in muscles with calculations of the oxygen pressure head necessary for supplying the tissue. *J. Physiol.* 52:409–415.

Lagerlund, T. D., and P. A. Low. 1987. A mathematical simulation of oxygen delivery in rat peripheral nerve. *Microvasc. Res.* 34:211–222.

Lentner, C. 1984. Geigy Scientific Tables. Ciba-Geigy Ltd., Switzerland. 99 pp.

Lochner, W., G. Arnold, and E. R. Müller-Ruchholtz. 1968. Metabolism of the artificially arrested heart and of the gas-perfused heart. *Am. J. Cardiol.* 22:299–311.

Loiselle, D. S. 1982. Stretch-induced increase in resting metabolism of isolated papillary muscle. *Biophys. J.* 38:185–194.

Loiselle, D. S. 1987. The effect of myoglobin-facilitated oxygen transport on the basal metabolism of papillary muscle. *Biophys. J.* 51: 905–913.

Loiselle, D. S. 1989. Exchange of oxygen across the epicardial surface distorts estimates of myocardial oxygen consumption. *J. Gen. Physiol.* 94:567–590.

Loock, J., and H. D. Schmidt. 1986. Relevance of oxygen diffusion loss through the surface in isolated hemoglobinfree perfused hearts. *Pflügers Arch.* 406:R32.

Mainwood, G. W., and K. Rakusan. 1982. A model for intracellular energy transport. *Can. J. Physiol. Pharmacol.* 60:98–102.

Mawson, D. A. 1991. A Model of the Oxygen Consumption of the Isolated, Saline-perfused Guinea-pig Heart. Master of Engineering Thesis, Department of Engineering Science, School of Engineering, University of Auckland, Auckland, New Zealand.

Moll, W. 1968. The diffusion coefficient of myoglobin in muscle homogenate. *Pflügers Arch.* 299:247–251.

Murray, J. D. 1974. On the role of myoglobin in muscle respiration. *J. Theoret. Biol.* 47:115–126.

Nichols, J. W., and L. J. Weber. 1989. Comparative oxygen affinity of fish and mammalian myoglobins. *J. Comp. Physiol.* B159:205–209.

Pennes, H. H. 1948. Analysis of tissue and arterial blood temperatures in the resting human forearm. *J. Appl. Physiol.* 1:93–122.

Piiper, J., M. Meyer, and P. Scheid. 1984. Dual role of diffusion in tissue gas exchange: blood-tissue equilibrium and diffusion shunt. *Resp. Physiol.* 56:131–144.

Piiper, J., and P. Scheid. 1986. Cross-sectional P_{O_2} distributions in Krogh cylinder and solid cylinder models. *Resp. Physiol.* 64:241–251.

Popel, A. S. 1981. Mathematical modeling of oxygen transport near a tissue surface: effect of the surface PO_2. *Math. Bio.* 55:231–246.

Popel, A. S., and J. F. Gross. 1979. Analysis of oxygen diffusion from arteriolar networks. *Am. J. Physiol.* 237:H681–H689.

Popel, A. S., R. N. Pittman, and M. L. Ellsworth. 1989. Rate of oxygen loss from arterioles is an order of magnitude higher than expected. *Am. J. Physiol.* 256:H921–H924.

Rossi-Fanelli, A., and E. Antonini. 1958. Studies on the oxygen and carbon

monoxide equilibria of human myoglobin. *Arch. Biochem. Biophys.* 77: 478–492.

Salathé, E. P., and R. W. Kolkka. 1986. Reduction of anoxia through myoglobin-facilitated diffusion of oxygen. *Biophys. J.* 50:885–894.

Schouten, V. J. A., C. P. Allaart, and N. Westerhof. 1992. Effect of perfusion pressure on force of contraction in thin papillary muscles and trabeculae from rat heart. *J. Physiol. (Lond.).* 451:585–604.

Stroeve, P. 1982. Myoglobin-facilitated oxygen transport in heterogeneous red muscle tissue. *Ann. Biomed. Eng.* 10:49–70.

Swain, D. P., and R. N. Pittman. 1989. Oxygen exchange in the microcirculation of hamster retractor muscle. *Am. J. Physiol.* 256: H247–H255.

Tateishi, N., N. Maeda, and T. Shiga. 1992. A method for measuring the rate of oxygen release from single microvessels. *Circ. Res.* 70: 812–819.

Taylor, B. A., and J. D. Murray. 1977. Effect of the rate of oxygen consumption on muscle respiration. *J. Math. Biol.* 4:1–20.

Theorell, H. 1934. Kristallinisches myoglobin. Die sauerstoffbindungskurve des myoglobins. *Biochemische Zeitschrift* 268:73–82.

Tota, B., V. Cimini, G. Salvatore, and G. Zummo. 1983. Comparative study of the arterial and lacunary systems of the ventricular myocardium of elasmobranch and teleost fishes. *Am. J. Anat.* 167:15–32.

van Beek, J. H. G. M., D. S. Loiselle, and N. Westerhof. 1992. Calculation of oxygen diffusion across the surface of isolated perfused hearts. *Am. J. Physiol.* 263:H1003–H1010.

van Ouwerkerk, H. J. 1977. Facilitated diffusion in a tissue cylinder with an anoxic region. *Pflügers Arch.* 372:221–230.

Wilson, D. F., M. Erecinska, C. Drown, and I. A. Silver. 1977. Effect of oxygen tension on cellular energetics. *Am. J. Physiol.* 233: C135–C140.